The Astrophysical Journal, 716:835–849, 2010 June 10 doi:10.1088/0004-637X/716/1/835


# *SUZAKU* OBSERVATIONS OF LUMINOUS QUASARS: REVEALING THE NATURE OF HIGH-ENERGY BLAZAR EMISSION IN LOW-LEVEL ACTIVITY STATES

A. A. Abdo[1,2], M. Ackermann[3], M. Ajello[3], E. Antolini[4,5], L. Baldini[6], J. Ballet[7], G. Barbiellini[8,9], M. G. Baring[10], D. Bastieri[11,12], K. Bechtol[3], R. Bellazzini[6], B. Berenji[3], R. D. Blandford[3], E. D. Bloom[3], E. Bonamente[4,5], A. W. Borgland[3], J. Bregeon[6], A. Brez[6], M. Brigida[13,14], P. Bruel[15], R. Buehler[3], S. Buson[11], G. A. Caliandro[16], R. A. Cameron[3], S. Carrigan[12], J. M. Casandjian[7], E. Cavazzuti[17], C. Cecchi[4,5], Ö. Çelik[18,19,20], A. Chekhtman[1,21], A. W. Chen[22], J. Chiang[3], S. Ciprini[5], R. Claus[3], J. Cohen-Tanugi[23], S. Colafrancesco[17], J. Conrad[24,25,65], S. Cutini[17], C. D. Dermer[1], F. de Palma[13,14], S. W. Digel[3], E. do Couto e Silva[3], P. S. Drell[3], R. Dubois[3], D. Dumora[26,27], C. Farnier[23], C. Favuzzi[13,14], S. J. Fegan[15], E. C. Ferrara[18], W. B. Focke[3], M. Frailis[28,29], Y. Fukazawa[30], P. Fusco[13,14], F. Gargano[14], D. Gasparrini[17], N. Gehrels[18], B. Giebels[15], N. Giglietto[13,14], P. Giommi[17], F. Giordano[13,14], M. Giroletti[31], T. Glanzman[3], G. Godfrey[3], P. Grandi[32], I. A. Grenier[7], L. Guillemot[26,27,33], S. Guiriec[34], D. Hadasch[35], A. K. Harding[18], M. Hayashida[3], D. Horan[15], R. E. Hughes[36], R. Itoh[30], M. S. Jackson[25,37], G. Jóhannesson[3], A. S. Johnson[3], W. N. Johnson[1], T. Kamae[3], H. Katagiri[30], J. Kataoka[38], N. Kawai[39,40], J. Knödlseder[41], M. Kuss[6], J. Lande[3], L. Latronico[6], F. Longo[8,9], F. Loparco[13,14], B. Lott[26,27], M. N. Lovellette[1], P. Lubrano[4,5], G. M. Madejski[3], A. Makeev[1,21], M. N. Mazziotta[14], J. E. McEnery[18,42], S. McGlynn[25,37], C. Meurer[24,25], P. F. Michelson[3], W. Mitthumsiri[3], T. Mizuno[30], C. Monte[13,14], M. E. Monzani[3], A. Morselli[43], I. V. Moskalenko[3], S. Murgia[3], I. Nestoras[33], P. L. Nolan[3], J. P. Norris[44], E. Nuss[23], T. Ohsugi[45], A. Okumura[46], E. Orlando[47], J. F. Ormes[44], M. Ozaki[48], D. Paneque[3], J. H. Panetta[3], D. Parent[1,21,26,27], V. Pelassa[23], M. Pepe[4,5], M. Pesce-Rollins[6], F. Piron[23], T. A. Porter[3], S. Rainò[13,14], R. Rando[11,12], M. Razzano[6], A. Reimer[3], O. Reimer[3], L. C. Reyes[49], A. Y. Rodriguez[16], M. Roth[50], F. Ryde[25,37], H. F.-W. Sadrozinski[51], R. Sambruna[18], A. Sander[36], R. Sato[48], C. Sgrò[6], M. S. Shaw[3], E. J. Siskind[52], P. D. Smith[36], G. Spandre[6], P. Spinelli[13,14], Ł. Stawarz[48,53], F. W. Stecker[18], M. S. Strickman[1], D. J. Suson[54], H. Takahashi[45], T. Takahashi[48], T. Tanaka[3], J. B. Thayer[3], J. G. Thayer[3], D. J. Thompson[18], O. Tibolla[55], D. F. Torres[16,35], G. Tosti[4,5], A. Tramacere[3,56,57], Y. Uchiyama[3], T. L. Usher[3], V. Vasileiou[19,20], N. Vilchez[41], M. Villata[58], V. Vitale[43,59], A. von Kienlin[47], A. P. Waite[3], P. Wang[3], B. L. Winer[36], K. S. Wood[1], Z. Yang[24,25], T. Ylinen[25,37,60], M. Ziegler[61], F. Tavecchio[56], M. Sikora[62], P. Schady[63], P. Roming[29], M. M. Chester[29], and L. Maraschi[64]

[1] Space Science Division, Naval Research Laboratory, Washington, DC 20375, USA
[2] National Research Council Research Associate, National Academy of Sciences, Washington, DC 20001, USA
[3] W. W. Hansen Experimental Physics Laboratory, Kavli Institute for Particle Astrophysics and Cosmology, Department of Physics and SLAC National Accelerator Laboratory, Stanford University, Stanford, CA 94305, USA
[4] Istituto Nazionale di Fisica Nucleare, Sezione di Perugia, I-06123 Perugia, Italy
[5] Dipartimento di Fisica, Università degli Studi di Perugia, I-06123 Perugia, Italy
[6] Istituto Nazionale di Fisica Nucleare, Sezione di Pisa, I-56127 Pisa, Italy
[7] Laboratoire AIM, CEA-IRFU/CNRS/Université Paris Diderot, Service d'Astrophysique, CEA Saclay, 91191 Gif sur Yvette, France
[8] Istituto Nazionale di Fisica Nucleare, Sezione di Trieste, I-34127 Trieste, Italy
[9] Dipartimento di Fisica, Università di Trieste, I-34127 Trieste, Italy
[10] Department of Physics and Astronomy, Rice University, MS-108, P.O. Box 1892, Houston, TX 77251, USA
[11] Istituto Nazionale di Fisica Nucleare, Sezione di Padova, I-35131 Padova, Italy
[12] Dipartimento di Fisica "G. Galilei," Università di Padova, I-35131 Padova, Italy
[13] Dipartimento di Fisica "M. Merlin" dell'Università e del Politecnico di Bari, I-70126 Bari, Italy
[14] Istituto Nazionale di Fisica Nucleare, Sezione di Bari, 70126 Bari, Italy
[15] Laboratoire Leprince-Ringuet, École polytechnique, CNRS/IN2P3, Palaiseau, France
[16] Institut de Ciencies de l'Espai (IEEC-CSIC), Campus UAB, 08193 Barcelona, Spain
[17] Agenzia Spaziale Italiana (ASI) Science Data Center, I-00044 Frascati (Roma), Italy
[18] NASA Goddard Space Flight Center, Greenbelt, MD 20771, USA
[19] Center for Research and Exploration in Space Science and Technology (CRESST) and NASA Goddard Space Flight Center, Greenbelt, MD 20771, USA
[20] Department of Physics and Center for Space Sciences and Technology, University of Maryland Baltimore County, Baltimore, MD 21250, USA
[21] George Mason University, Fairfax, VA 22030, USA
[22] INAF-Istituto di Astrofisica Spaziale e Fisica Cosmica, I-20133 Milano, Italy
[23] Laboratoire de Physique Théorique et Astroparticules, Université Montpellier 2, CNRS/IN2P3, Montpellier, France
[24] Department of Physics, Stockholm University, AlbaNova, SE-106 91 Stockholm, Sweden
[25] The Oskar Klein Centre for Cosmoparticle Physics, AlbaNova, SE-106 91 Stockholm, Sweden
[26] CNRS/IN2P3, Centre d'Études Nucléaires Bordeaux Gradignan, UMR 5797, Gradignan 33175, France
[27] Université de Bordeaux, Centre d'Études Nucléaires Bordeaux Gradignan, UMR 5797, Gradignan 33175, France
[28] Dipartimento di Fisica, Università di Udine and Istituto Nazionale di Fisica Nucleare, Sezione di Trieste, Gruppo Collegato di Udine, I-33100 Udine, Italy
[29] Osservatorio Astronomico di Trieste, Istituto Nazionale di Astrofisica, I-34143 Trieste, Italy
[30] Department of Physical Sciences, Hiroshima University, Higashi-Hiroshima, Hiroshima 739-8526, Japan
[31] INAF Istituto di Radioastronomia, 40129 Bologna, Italy
[32] INAF-IASF Bologna, 40129 Bologna, Italy
[33] Max-Planck-Institut für Radioastronomie, Auf dem Hügel 69, 53121 Bonn, Germany
[34] Center for Space Plasma and Aeronomic Research (CSPAR), University of Alabama in Huntsville, Huntsville, AL 35899, USA
[35] Institució Catalana de Recerca i Estudis Avançats (ICREA), Barcelona, Spain
[36] Department of Physics, Center for Cosmology and Astro-Particle Physics, The Ohio State University, Columbus, OH 43210, USA
[37] Department of Physics, Royal Institute of Technology (KTH), AlbaNova, SE-106 91 Stockholm, Sweden
[38] Research Institute for Science and Engineering, Waseda University, 3-4-1, Okubo, Shinjuku, Tokyo 169-8555, Japan
[39] Department of Physics, Tokyo Institute of Technology, Meguro City, Tokyo 152-8551, Japan

[40] Cosmic Radiation Laboratory, Institute of Physical and Chemical Research (RIKEN), Wako, Saitama 351-0198, Japan
[41] Centre d'Étude Spatiale des Rayonnements, CNRS/UPS, BP 44346, F-30128 Toulouse Cedex 4, France
[42] Department of Physics and Department of Astronomy, University of Maryland, College Park, MD 20742, USA
[43] Istituto Nazionale di Fisica Nucleare, Sezione di Roma "Tor Vergata," I-00133 Roma, Italy
[44] Department of Physics and Astronomy, University of Denver, Denver, CO 80208, USA
[45] Hiroshima Astrophysical Science Center, Hiroshima University, Higashi-Hiroshima, Hiroshima 739-8526, Japan
[46] Department of Physics, Graduate School of Science, University of Tokyo, 7-3-1 Hongo, Bunkyo-ku, Tokyo 113-0033, Japan
[47] Max-Planck Institut für extraterrestrische Physik, 85748 Garching, Germany
[48] Institute of Space and Astronautical Science, JAXA, 3-1-1 Yoshinodai, Sagamihara, Kanagawa 229-8510, Japan; rsato@astro.isas.jaxa.jp
[49] Institut für Astro- und Teilchenphysik and Institut für Theoretische Physik, Leopold-Franzens-Universität Innsbruck, A-6020 Innsbruck, Austria
[50] Kavli Institute for Cosmological Physics, University of Chicago, Chicago, IL 60637, USA
[51] Department of Physics, University of Washington, Seattle, WA 98195-1560, USA
[52] NYCB Real-Time Computing Inc., Lattingtown, NY 11560-1025, USA
[53] Astronomical Observatory, Jagiellonian University, 30-244 Kraków, Poland
[54] Department of Chemistry and Physics, Purdue University Calumet, Hammond, IN 46323-2094, USA
[55] Institut für Theoretische Physik and Astrophysik, Universität Würzburg, D-97074 Würzburg, Germany
[56] Consorzio Interuniversitario per la Fisica Spaziale (CIFS), I-10133 Torino, Italy
[57] INTEGRAL Science Data Centre, CH-1290 Versoix, Switzerland
[58] INAF, Osservatorio Astronomico di Torino, I-10025 Pino Torinese (TO), Italy
[59] Dipartimento di Fisica, Università di Roma "Tor Vergata," I-00133 Roma, Italy
[60] School of Pure and Applied Natural Sciences, University of Kalmar, SE-391 82 Kalmar, Sweden
[61] Santa Cruz Institute for Particle Physics, Department of Physics and Department of Astronomy and Astrophysics, University of California at Santa Cruz, Santa Cruz, CA 95064, USA
[62] Nicolaus Copernicus Astronomical Center, Bartycka 18, 00-716, Warsaw, Poland
[63] Mullard Space Science Laboratory/UCL, Holmbury St. Mary, Dorking, Surrey RH5 6NT, UK
[64] Osservatorio Astronomico di Brena, via Brera, 28, Milano I-20121, Italy
*Received 2009 December 24; accepted 2010 April 10; published 2010 May 21*

## ABSTRACT

We present the results from the *Suzaku* X-ray observations of five flat-spectrum radio quasars (FSRQs), namely PKS 0208−512, Q 0827+243, PKS 1127−145, PKS 1510−089, and 3C 454.3. All these sources were additionally monitored simultaneously or quasi-simultaneously by the *Fermi* satellite in gamma rays and the *Swift* UVOT in the UV and optical bands, respectively. We constructed their broadband spectra covering the frequency range from $10^{14}$ Hz up to $10^{25}$ Hz, and those reveal the nature of high-energy emission of luminous blazars in their low-activity states. The analyzed X-ray spectra are well fitted by a power-law model with photoelectric absorption. In the case of PKS 0208−512, PKS 1127−145, and 3C 454.3, the X-ray continuum showed indication of hardening at low energies. Moreover, when compared with the previous X-ray observations, we see a significantly increasing contribution of low-energy photons to the total X-ray fluxes when the sources are getting fainter. The same behavior can be noted in the *Suzaku* data alone. A likely explanation involves a variable, flat-spectrum component produced via inverse-Compton emission, plus an additional, possibly steady soft X-ray component prominent when the source gets fainter. This soft X-ray excess is represented either by a steep power-law (photon indices $\Gamma \sim 3$–5) or a blackbody-type emission with temperatures $kT \sim 0.1$–0.2 keV. We model the broadband spectra of the five observed FSRQs using synchrotron self-Compton and/or external-Compton radiation models. Our modeling suggests that the difference between the low- and high-activity states in luminous blazars is due to the different total kinetic power of the jet, most likely related to varying bulk Lorentz factor of the outflow within the blazar emission zone.

*Key words:* galaxies: active – galaxies: jets – radiation mechanisms: non-thermal – X-rays: galaxies

*Online-only material:* color figures

## 1. INTRODUCTION

Observations with the EGRET instrument (30 MeV to 30 GeV; Thompson et al. 1993) on board the *Compton Gamma-Ray Observatory* have resulted in detection of $\gamma$-ray emission from a few hundred astrophysical sources, 66 of which were securely associated with active galactic nuclei (AGNs; e.g., Hartman et al. 1999). Most of the AGNs detected by EGRET show characteristics of the blazar class. Observationally, this class includes flat-spectrum radio quasars (FSRQs) and BL Lac objects. FSRQs have strong and broad optical emission lines, while the lines are weak or absent in BL Lacs. During the first three months of the *Fermi* Large Area Telescope's (LAT) all-sky-survey, 132 bright sources at high Galactic latitudes ($|b| > 10^{\circ}$) were detected at a confidence level greater than $10\sigma$ (Abdo et al. 2009a). As expected from the EGRET observations, a large fraction (106) of these sources have been associated with known AGNs (Abdo et al. 2009b). This includes two radio galaxies (Centaurus A and NGC 1275; Abdo et al. 2009c) and 104 blazars consisting of 58 FSRQs, 42 BL Lac objects, and 4 blazars with unknown classification based on their spectral energy distribution (SED).

The radio-to-optical emission of luminous blazars of the FSRQ type is known to be produced by the synchrotron radiation of relativistic electrons accelerated within the outflow, while the inverse-Compton (IC) scattering of low-energy photons by the same relativistic electrons is most likely responsible for the formation of the high-energy X-ray-to-$\gamma$-ray component. In addition, it is widely believed that the IC emission from FSRQs is dominated by the scattering of soft photons external to the jet (external Compton radiation (ECR)). These photons, in turn, are

[65] Royal Swedish Academy of Sciences Research Fellow, funded by a grant from the K. A. Wallenberg Foundation.

**Table 1**
*Suzaku* Observation Log of Five FSRQs

| Object | $z$ | Start Time (UT) | Stop Time (UT) | XIS/HXD Exposures (ks) |
|---|---|---|---|---|
| 0208−512 | 1.003 | 2008 Dec 14 07:33 | 2008 Dec 15 11:30 | 50.3/39.3 |
| 0827+243 | 0.939 | 2008 Oct 27 05:11 | 2008 Oct 28 08:04 | 35.3/36.3 |
| 1127−145 | 1.187 | 2008 Nov 29 18:10 | 2008 Nov 30 22:51 | 42.2/29.0 |
| 1510−089 | 0.361 | 2009 Jan 27 04:32 | 2009 Jan 28 05:25 | 38.5/36.2 |
| 3C 454.3 | 0.859 | 2008 Nov 22 09:19 | 2008 Nov 23 16:31 | 39.9/40.4 |

produced by the accretion disk, and interact with the jet either directly or indirectly, after being scattered or reprocessed in the broad-line region (BLR) or a dusty torus (DT; see, e.g., Dermer & Schlickeiser 1993; Sikora et al. 1994; Błażejowski et al. 2000). Other sources of seed photons can also contribute to the observed IC radiation, and these are in particular jet synchrotron photons through the synchrotron self-Compton process (SSC; Maraschi et al. 1992; Sokolov & Marscher 2005).

In this context, detailed X-ray studies offer a unique possibility for discriminating between different proposed jet emission models, since those scenarios predict distinct components to be prominent in blazar spectra around keV photon energies. For example, in the soft X-ray range a break is expected in the ECR/BLR model, tracking the low-energy end of the electron energy distribution (Tavecchio et al. 2000; Sikora et al. 2009). Indeed, both the *XMM-Newton* and the *Suzaku* X-ray data of RBS 315 show "convex" spectra (Tavecchio et al. 2007). Such a curvature, on the other hand, can be alternatively accounted for by an excess absorption below 1 keV over the Galactic value, or by an intrinsic curvature in the electron energy distribution. Furthermore, the situation can be more complex, with the simultaneous presence of yet additional components, such as the high-energy tail of the synchrotron continuum, SSC emission, or the narrow-band spectral feature originating from the "bulk Comptonization" of external UV (disk) radiation by cold electrons within the innermost parts of relativistic outflow (Begelman & Sikora 1987; Sikora & Madejski 2000; Moderski et al. 2004; Celotti et al. 2007).

Ghisellini et al. (1998) have studied the SED of 51 EGRET-detected $\gamma$-ray loud blazars and have applied the SSC+ECR model to the spectra of these sources. Although most of the broadband data collected by Ghisellini et al (1998) corresponded to non-simultaneous measurements, those authors discovered clear trends and correlations among the physical quantities obtained from the model calculations. In particular, they found an evidence for a well-defined sequence such that the observed spectral properties of different blazar classes (BL Lacs and FSRQs) can be explained by an increasing contribution of an external radiation field toward cooling jet electrons (thus producing the high-energy emission) with the increasing jet power. As a result, while the SSC process alone may account for the entire high-energy emission of low-power sources (BL Lacs), a significant contribution from the ECR is needed to explain the observed spectra of high-power blazars (FSRQs). Meanwhile, when focusing on one particular object, Mukherjee et al. (1999) reported that they found a similar trend in the different spectral states of PKS 0528+134. They studied the sequence of flaring and low-flux states of the source and found that the SSC mechanism plays a more important role when the source is in a low state, and the ECR mechanism is the dominant electron cooling mechanism when the source is in a high $\gamma$-ray state (see in this context also Sambruna et al. 1997).

In order to understand the blazar phenomenon and the differences between BL Lacs and FSRQs, as well as the origin of spectral transitions in a particular object, one has to obtain truly simultaneous coverage across the entire spectrum, during both flaring and low-activity states. However, past $\gamma$-ray observations in low-activity states have been limited to only a few extremely luminous objects, such as PKS 0528−134 or 3C 279. Only now, with the successful launch of the *Fermi* satellite and the excellent performance of the *Suzaku* instruments, we do have an opportunity to study high-energy spectra of blazars with substantially improved sensitivity, and therefore can probe the different states of the sources' activity.

In this paper, we report the high-sensitivity, broadband *Suzaku* observations of five FSRQs, namely PKS 0208−512, Q 0827+243, PKS 1127−145, PKS 1510−089, and 3C 454.3, which were bright gamma-ray sources detected by EGRET. Additionally, all of these sources were monitored simultaneously or quasi-simultaneously by the *Fermi* LAT and *Swift* Ultraviolet/Optical Telescope (UVOT; Roming et al. 2005). These broadband and high-sensitivity observations allow us to reveal the characteristics of the high-energy IC continuum in the low-activity states of luminous blazars. The paper is organized as follows: in Section 2, we describe observation and data reduction in the X-ray (*Suzaku*), UV-optical (*Swift* UVOT), and $\gamma$-ray (*Fermi* LAT) domains. In Section 3, we present the broadband analysis results. Finally, in Section 4 we discuss the constraints on the jet parameters and speculate on the the origin of different activity states in luminous blazars. Throughout the paper we adopt the cosmological parameters $H_0 = 71$ km s$^{-1}$ Mpc$^{-1}$, $\Omega_{\rm M} = 0.27$, and $\Omega_\Lambda = 0.73$.

## 2. OBSERVATION AND DATA REDUCTION

### 2.1. Suzaku

Five FSRQs were observed by *Suzaku* (Mitsuda et al. 2007) for 40 ks each as one of the long-category projects between 2008 October and 2009 January. Table 1 summarizes the start time, end time, and the exposures for each observation. *Suzaku* carries four sets of X-ray telescopes (Serlemitsos et al. 2007), each with a focal-plane X-ray CCD camera (XIS, X-ray Imaging Spectrometer; Koyama et al. 2007) that is sensitive over the 0.3–12 keV band, together with a non-imaging Hard X-ray Detector (HXD; Takahashi et al. 2007; Kokubun et al. 2007), which covers the 10–600 keV energy band by utilizing Si PIN photo-diodes and GSO scintillation detectors. All of the sources were focused on the nominal center position of the XIS detectors.

For the XIS, we used data sets processed using the software of the *Suzaku* data processing pipeline (ver. 2.2.11.22). Reduction and analysis of the data were performed following the standard procedure using the HEADAS v6.5 software package. The screening was based on the following criteria: (1) only

**Table 2**
*Swift* Observation Log of Five FSRQs

| Object | ObsID | Start Time (UT) | Exposure[a] (ks) | Exposure[b] (ks) | Filter[b] |
|---|---|---|---|---|---|
| 0208−512 | 00035002024 | 2008 Dec 14 15:25 | 0.99 | 0.94 | All |
| 0827+243 | 00036375004 | 2008 Dec 8 13:42 | 1.72 | 1.71 | *u* |
| 1127−145 | 00036380001 | 2007 Mar 24 00:32 | 14.6 | 14.2 | All |
| 1510−089 | 00031173010 | 2009 Jan 25 18:40 | 3.46 | 3.40 | *u*, w1, m2 |
| 3C 454.3 | 00035030030 | 2008 Oct 26 20:28 | 0.43 | 0.40 | All |

**Notes.**
[a] *Swift* XRT.
[b] *Swift* UVOT.

ASCA-grade 0, 2, 3, 4, 6 events were accumulated, while hot and flickering pixels were removed using the CLEANSIS script, (2) the time interval after the passage of South Atlantic Anomaly was greater than 500 s, and (3) the object was at least 5° and 20° above the rim of the Earth (ELV) during night and day, respectively. In addition, we also selected the data with a cutoff rigidity (COR) larger than 6 GV. The XIS events were extracted from a circular region with a radius of 4.′2 centered on the source peak, whereas the background was accumulated in an annulus with inner and outer radii of 5.′4 and 7.′3, respectively. We checked that the use of different source and background regions did not affect the analysis results. The response and auxiliary files were produced using the analysis tools XISRMFGEN and XISSIMARFGEN developed by the *Suzaku* team, which are included in the software package HEAsoft version 6.5.

The HXD/PIN data (version 2.0) were processed with basically the same screening criteria as those for the XIS, except that we required ELV $\geqslant 5^\circ$ through night and day and COR $\geqslant 8$ GV. The HXD/PIN instrumental background spectra were provided by the HXD team for each observation (Kokubun et al. 2007; Fukazawa et al. 2006). Both the source and background spectra were made with identical good time intervals and the exposure was corrected for detector dead time of 6.0%–8.0%. We used the response files, version AE_HXD_PINHXDNOM5_20080716.RSP, provided by the HXD team. In our analysis, the hard X-ray emission of PKS 1510−089 and 3C454.3 were detected in the energy range from 12 keV to 40 keV and 50 keV, respectively. For other objects, the sources were not detected in the HXD/PIN data. We also note here that for all of the objects, the sources were not detected in the HXD/GSO data.

### 2.2. *Swift*

Four analyzed FSRQs (PKS 0208−512, Q 0827+243, PKS 1510−089, and 3C 454.3) were observed with *Swift* between 2008 October and 2009 January, as part of *Swift* "target of opportunity" observations. We analyzed the data taken within or near the time of the *Suzaku* observations. For the case of PKS 1127−145, however, the observations were made only once in 2007 March. We focused on analysis of the UVOT data, since *Suzaku* provides much better photon statistics in X-rays than the *Swift* X-ray Telescope (XRT; Burrows et al. 2005) and Burst Alert Telescope (BAT; Barthelmy et al. 2005), thanks to the long *Suzaku* exposures. We used the XRT data primarily for a consistency check regarding the spectral properties. Table 2 summarizes the start time, exposure time, and filters used for each observation.

The UVOT observing mode commonly takes an exposure in each of the six optical and ultraviolet filters ($v$, $b$, $u$, uvw1, uvm2, and uvw2) per *Swift* pointing. The list of UVOT observations is given in Table 2. For the screening, reduction, and analysis of the *Swift* data, we used standard procedures within the HEASoft v.6.5 software package with the calibration database updated as of 2009 February 28. For this analysis, Level 2 sky-corrected image data were used. Since all sources were relatively bright, the source aperture sizes were chosen to correspond to those used to determine the UVOT zero points: 5″ for the optical and UV filters (Poole et al. 2008). The background was extracted from a nearby source-free circular region with 15″ radius. All image data were corrected for coincidence loss. The observed magnitudes were converted into flux densities by the standard procedures (Poole et al. 2008).

The XRT data were all taken in Photon Counting mode (PC mode; Hill et al. 2004). The data were reduced by the XRT data analysis task XRTPIPLINE version 0.12.0. Photons were selected from the event file by xselect version 2.4. The auxiliary response file was created by the XRT task XRTMKARF and the standard response file SWXPC0TO12S6_20010101V011.RMF. All spectra were analyzed in the 0.3–10.0 keV band using XSPEC version 11.3.2.

### 2.3. *Fermi LAT*

During the first year of *Fermi* LAT (Atwood et al. 2009) operation, most of the telescope's time has been dedicated to "survey mode" observing, where *Fermi* points away from the Earth, and nominally rocks the spacecraft axis north and south from the orbital plane to enable monitoring of the entire sky every ∼3 hr (or 2 orbits). We analyzed the LAT's observations of the five blazar regions using data collected during the first 4–5 months centered around *Suzaku* observations. Little variability indicated by the LAT light curves for the studied objects during this time implies that the constructed broadband spectra, even though not exactly simultaneous, are representative for the low-activity states of all five blazars.

The data used here comprise all scientific data obtained between 4 August and 2008 December 19 for PKS 0208−512, Q 0827+243, PKS 1127−145, and 3C 454.3 (interval runs from Mission Elapsed Time (MET) 239557417 to 251345942), and 2008 August 4 and 2009 January 30 for 1510−089 (MET 239557417 to 254966035), respectively. We have applied the zenith angle cut to eliminate photons from Earth's limb, at 105°. This is important in pointed mode observations, but also important for survey mode due to overshoots and Sun avoidance maneuvers. In addition, we excluded the time intervals when the rocking angle was more than 43°. We use the "Diffuse" class events (Atwood et al. 2009), which, of all reconstructed events have the highest probability of being photons.

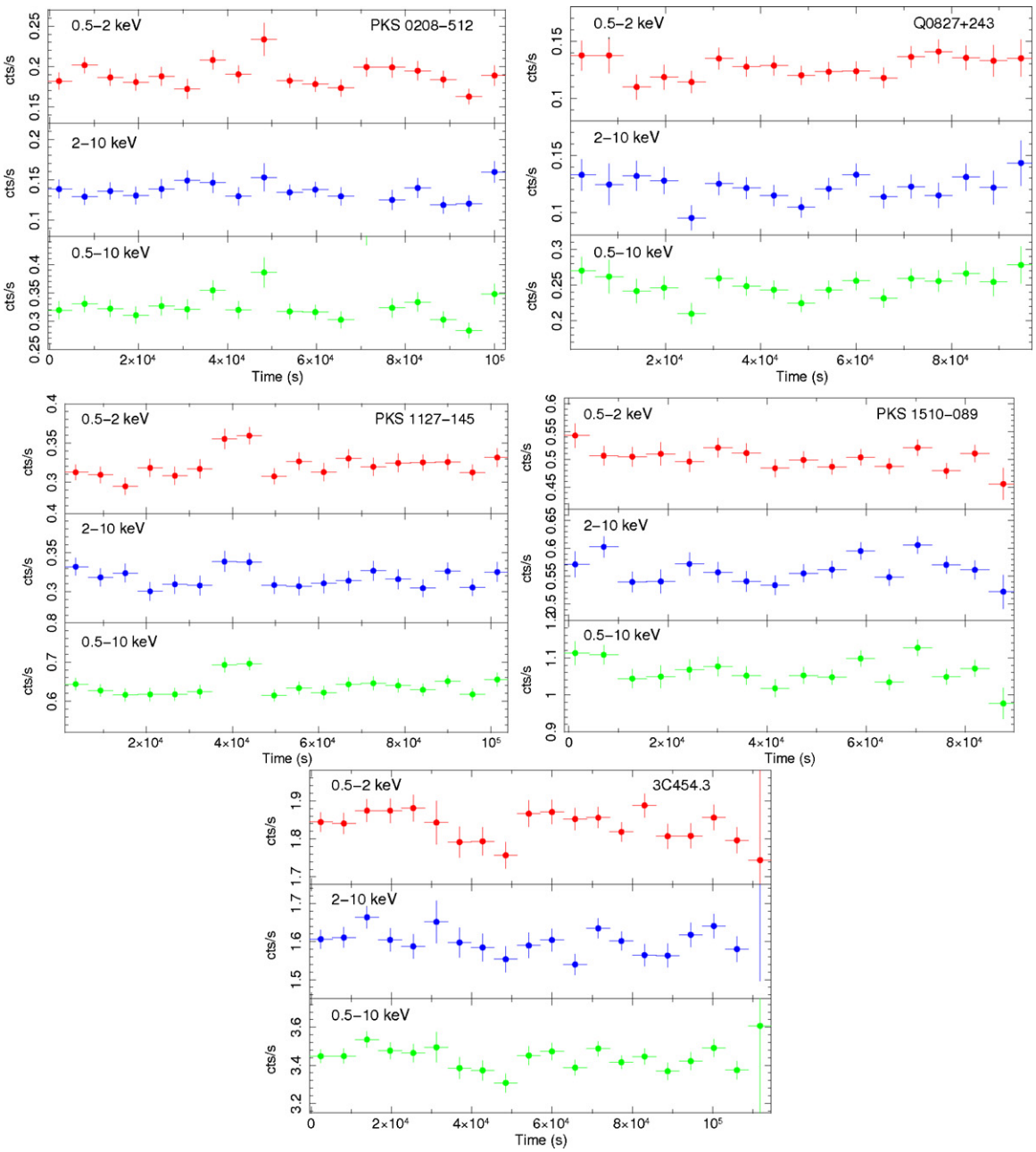


**Figure 1.** Light curves of five FSRQs: 0.5–2 keV (upper panels), 2–10 keV (middle panels), and 0.5–10 keV (bottom panels). All the light curves were binned at 5760 s, corresponding to the period of the *Suzaku* orbit.

(A color version of this figure is available in the online journal.)

In the analysis presented here, we set the lower energy bound to a value of 200 MeV, since the bin counts for photons with energies of ∼100 MeV and lower are systematically lower than expected based on extrapolations of reasonable functions. Science Tools version v9r14 and instrumental response functions (IRFs) P6_V3 were used.

## 3. RESULTS

### *3.1. Suzaku*

#### *3.1.1. Temporal Analysis*

Figure 1 shows the count rate variations of the five observed FSRQs. The summed XISs (XIS0,1,3) light curves are shown separately in different energy bands: 0.5–2 keV (upper panel), 2–10 keV (middle panel), and 0.5–10 keV (bottom panel), respectively. Since the count rate variations of the HXD/PIN detector were less clear due to limited photon statistics and uncertainty of the modeling of the non-X-ray background, we only concentrate on the temporal variability of the XIS data below 10 keV. We evaluate the fractional variability by calculating the variability amplitude relative to the mean count rate corrected for effects of random errors (e.g., Edelson et al. 2001): $F_{\rm var} = \sqrt{S^2 - \overline{\sigma_{\rm err}}^2}/\overline{x}$, where $S^2$ is the total variance of the light curve, $\overline{\sigma_{\rm err}}^2$ is the mean error squared, and $\overline{x}$ is the mean count rate. The variability amplitude in the XIS bands are $F_{\rm var} = 0.036 \pm 0.021$ for 0208−512, $F_{\rm var} = 0.027 \pm 0.010$ for 1127−145, and $F_{\rm var} = 0.025 \pm 0.008$ for 1510−089, respectively. 0827+243 and 3C454.3 show only weak variability, which is not significant.

**Table 3**
Results of the Spectral Fits to the *Suzaku* Data Using a Power Law with Galactic Absorption

| Object | $N_H$[a] | $\Gamma$ | $F_{2-10\,keV}$[b] | Constant (XIS0,1,3,HXD/PIN) | $\chi^2_r$ (dof) |
|---|---|---|---|---|---|
| 0208−512 | 3.08 (fixed) | 1.68 ± 0.03 | 1.37 ± 0.06 | 1,1.04 ± 0.05,1.04 ± 0.05,None | 0.91 (250) |
| 0827+243 | 3.62 (fixed) | 1.46 ± 0.04 | 1.37 ± 0.07 | 1,0.90 ± 0.05,1.04 ± 0.06,None | 0.84 (194) |
| 1127−145 | 3.83 (fixed) | 1.41 ± 0.02 | 3.45 ± 0.08 | 1,1.03 ± 0.03,1.05 ± 0.03,None | 1.01 (331) |
| 1510−089 | 7.88 (fixed) | 1.37 ± 0.01 | 6.31 ± 0.12 | 1,1.00 ± 0.02,1.02 ± 0.02,1.13 | 1.06 (407) |
| 3C 454.3 | 7.24 (fixed) | 1.58 ± 0.01 | 16.7 ± 0.2 | 1,1.04 ± 0.01,1.02 ± 0.01,1.13 | 1.00 (1090) |

**Notes.** Errors correspond to 90% confidence level.
[a] Fixed value indicates the Galactic absorption column density in units of $10^{20}$ cm$^{-2}$.
[b] Flux in units of $10^{-12}$ erg cm$^{-2}$ s$^{-1}$.

**Table 4**
Results of the Spectral Fits to the *Suzaku* Data with Best-fit Models

| Object | Model[a] | $N_H$ | $\Gamma_{hi}$[b] | $\Gamma_{low}$[c] | $F_{2-10\,keV}$[d] | kT (keV) | $\chi^2_r$ |
|---|---|---|---|---|---|---|---|
| 0208−512 | PL | 3.08 (fixed) | 1.68 ± 0.03 | ... | 1.37 ± 0.06 | ... | 0.91 (250) |
| 0827+243 | PL | 3.62 (fixed) | 1.46 ± 0.04 | ... | 1.37 ± 0.07 | ... | 0.84 (194) |
| 1127−145 | PL | $10.8^{+1.6}_{-1.5}$ | 1.52 ± 0.03 | ... | 3.36 ± 0.08 | ... | 0.82 (330) |
| 1510−089 | PL+BB | 7.88 (fixed) | 1.32 ± 0.03 | ... | 6.42 ± 0.13 | 0.15 ± 0.03 | 0.97 (405) |
| | PL+PL | 7.88 (fixed) | $1.26^{+0.06}_{-0.12}$ | $2.85^{+0.88}_{-0.40}$ | $6.30^{+0.18}_{-0.74}$ | ... | 0.96 (405) |
| 3C 454.3 | PL | $9.07^{+0.58}_{-0.57}$ | 1.62 ± 0.01 | ... | 16.6 ± 0.2 | ... | 0.97 (1089) |

**Notes.**
[a] Spectral fitting models. PL, power-law function; PL+PL, double power-law function; PL+BB, power-law + blackbody model.
[b] Differential spectral photon index.
[c] Differential spectral photon index at the low-energy X-ray band, when fitted with a double power-law function.
[d] Flux in units of $10^{-12}$ erg cm$^{-2}$ s$^{-1}$.

### *3.1.2. Time-averaged Spectral Analysis*

In the following we report the analysis procedure and results for each object. The background-subtracted spectra were fitted using XSPEC ver.11.3.2. All errors are quoted at the 90% confidence level for the parameter of interest unless otherwise stated. All the fits in this paper are restricted to the energy ranges of 0.5–10 keV (XIS0,3: the FI chips), 0.3–8 keV (XIS1: the BI chip), 12–40 keV for PKS 1510−089, and 12–50 keV for 3C 454.3 (HXD/PIN). We fixed the relative normalization of the XISs and HXD/PIN at 1.13, which is carefully determined from the XIS calibration using nominal pointings of the Crab Nebula. Serlemitsos et al. (2007) reported that spectral normalizations are slightly different (a few percent) among the CCD sensors based on a contemporaneous fit of the Crab spectra. Therefore, we adjusted the normalization factor among the three XISs relative to XIS0. The results of the spectral fits with a simple absorbed power-law model are summarized in Table 3 (with Galactic absorption) and Table 4.

*PKS 0208−512.* The time-averaged, background subtracted three XIS spectra of PKS 0208−512, when fitted jointly, are well described by a single absorbed power-law model, and the absorption column is consistent with the Galactic value $N_H = 3.08 \times 10^{20}$ cm$^{-2}$ (Dickey & Lockman 1990). We obtained the best-fit photon index $\Gamma = 1.68 \pm 0.03$ and the 2–10 keV flux $F_{2-10\,keV} = (1.37 \pm 0.06) \times 10^{-12}$ erg cm$^{-2}$ s$^{-1}$ with a chi-squared value of 0.91 for 250 degrees of freedom (dof). Figure 2 shows the spectra obtained with the XISs with residuals plotted against the best-fit power-law model with Galactic absorption. Although statistically acceptable, we notice that the residuals of the fits show moderate excess feature at low energies, below 1 keV.

In the previous observation with BeppoSAX during a high flux state (Tavecchio et al. 2002), $F_{2-10\,keV} \sim 4.7 \times 10^{-12}$ erg cm$^{-2}$ s$^{-1}$, which is a factor of 3 larger than in our *Suzaku* observations, the X-ray spectrum is well described by a power law with photon index $\Gamma \sim 1.7$, similar to the *Suzaku* result. However, Tavecchio et al. reported that the spectrum was heavily absorbed below 1 keV, indicating a column density of $N_H = 1.67 \times 10^{21}$ cm$^{-2}$. Figure 3 shows the *Suzaku* spectrum with residuals assuming such an increased value of $N_H$. The residuals indicate significant soft excess emission below 1 keV, if $N_H$ is the same as found in the previous BeppoSAX observation.

The variable soft X-ray emission of PKS 0208−512 may indicate that the convex spectrum observed by BeppoSAX reflects an intrinsic IC continuum shape, while the soft excess observed by *Suzaku* reflects the presence of an additional spectral component which becomes prominent when the source gets fainter (see Tavecchio et al. 2007; Kataoka et al. 2008). Therefore, to model in more detail the observed X-ray spectrum, we first considered a double power-law fit (PL + PL) in which the soft X-ray excess is represented by a steep power-law component. The absorption column is fixed at $N_H = 1.67 \times 10^{21}$ cm$^{-2}$, as given by Tavecchio et al. (2002). We obtained the photon indices $\Gamma_1 = 4.98^{+0.56}_{-0.53}$ and $\Gamma_2 = 1.71 \pm 0.07$. This provides an acceptable fit, with $\chi^2_r$/dof = 0.90/248. We also considered an alternative fit consisting of a power-law function and a blackbody component. This model also gives a similarly good representation of the data with $\chi^2_r$/dof = 0.90/248, implying $\Gamma = 1.78 \pm 0.04$ and the temperature of the introduced thermal component of $kT = 0.093 \pm 0.004$ keV. Both fits appear to be as good as a single power law with free absorption, and do not improve the goodness of fit.

*Q 0827+243.* The time-averaged spectra of Q 0827+243 collected with the XISs are well fitted by an absorbed power-law model with a photon index $\Gamma = 1.46 \pm 0.04$ ($\chi^2_r = 0.84$ for

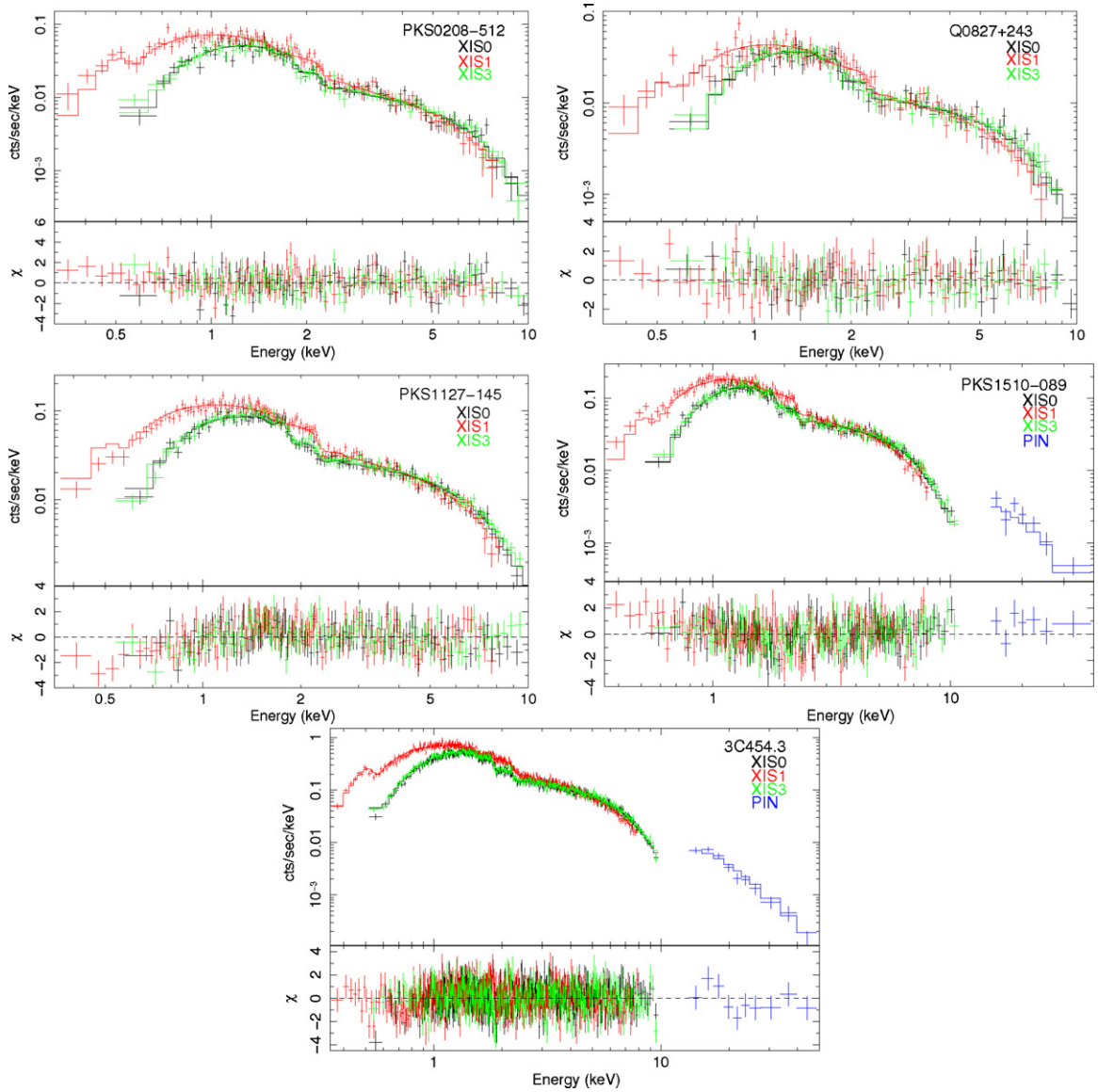


**Figure 2.** *Suzaku* spectra of five FSRQs: the top panel shows the data, plotted against a power-law model with the Galactic absorption. The bottom panel shows the residuals for the power-law fit. For 0208−512 and 1510−089, the data below 1 keV are in excess to the model. On the other hand, for 1127−145, the residuals show a substantial deficit of photons at low energies. For 3C454.3, some scatter around 1 keV in the residual panel is seen.

(A color version of this figure is available in the online journal.)

194 dof). The absorption column is consistent with the Galactic value of $N_{\rm H} = 3.62 \times 10^{20}$ cm$^{-2}$ (Dickey & Lockman 1990), and the flux over 2–10 keV is $F_{2-10\,{\rm keV}} = (1.37 \pm 0.07) \times 10^{-12}$ erg cm$^{-2}$ s$^{-1}$. As shown in Figure 2, there is no evidence for any additional spectral feature in the soft band. This result is in good agreement with previous *Chandra* observations of the core (Jorstad & Marscher 2004), revealing that the X-ray continuum is well described by a power-law model ($\Gamma \sim 1.4$) with Galactic absorption.

*PKS 1127−145.* We first fitted the XISs spectra with a single power-law model with a Galactic absorption of $N_{\rm H} = 3.83 \times 10^{20}$ cm$^{-2}$ (Murphy et al. 1996). We obtained the photon index of $\Gamma = 1.41 \pm 0.02$ $\chi^2_{\rm r} = 1.01$ for 331 dof), but the residuals show a substantial deficit of photons at low energies (Figure 2). To investigate this deficit in more detail, we fitted the spectra with a single power-law and a free absorption model. This model represents well the spectra with the best chi-squared value of 0.82 for 330 dof (Figure 4), indicating that the column density is higher than the Galactic value at the 99.9% confidence level. For this model the photon index is $\Gamma = 1.51 \pm 0.03$ and the unabsorbed X-ray flux is $F_{2-10\,{\rm keV}} = (3.36 \pm 0.08) \times 10^{-12}$ erg cm$^{-2}$ s$^{-1}$. The best-fit column density is $N_{\rm H} = (1.08^{+1.6}_{-1.5}) \times 10^{21}$ cm$^{-2}$, which is similar to the one found in previous *Chandra* and *XMM-Newton* observations ($N_{\rm H} \sim 1.2 \times 10^{21}$ cm$^{-2}$) during a high state with $F_{2-10\,{\rm keV}} \sim 6 \times 10^{-12}$ erg cm$^{-2}$ s$^{-1}$ (Bechtold et al. 2001; Foschini et al. 2006). We note that the Galactic absorption and a broken power-law model also well represent the spectra with $\chi^2_{\rm r}$/dof of 0.81/329. In this model, the spectrum below $E_{\rm brk} = 1.50 \pm 0.13$ keV is rather hard ($\Gamma_1 = 1.10 \pm 0.08$), and the high-energy photon index is $\Gamma_2 = 1.50 \pm 0.03$.

*PKS 1510−089.* Figure 2 shows the XISs and HXD/PIN spectra of PKS 1510−089 (including residuals), plotted against the best-fit power-law model with Galactic absorption, using the overall X-ray data between 0.3 and 40 keV. The best-fit photon index is $\Gamma = 1.37 \pm 0.01$ and the unabsorbed X-ray flux is

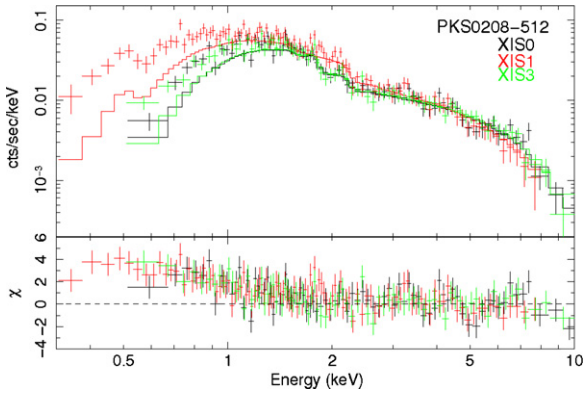


**Figure 3.** *Suzaku* spectrum of PKS 0208−512, with residuals assuming a column density of $N_{\rm H} \sim 1.67 \times 10^{21}$ cm$^{-2}$. Deviations due to soft excess emission can be clearly seen.

(A color version of this figure is available in the online journal.)

$F_{2-10\,\rm keV} = (6.31 \pm 0.12) \times 10^{-12}$ erg cm$^{-2}$ s$^{-1}$. However, this model did not represent the spectra well, yielding a chi-squared value of 1.06 for 407 dof. The residuals indicate some excess emission at low energies.

To represent the observed X-ray spectra, we tried the same analysis as for PKS 0208−512. We first fitted the data by a double power-law model with Galactic absorption. We obtained the photon indices $\Gamma_1 = 2.85^{+0.88}_{-0.40}$ and $\Gamma_2 = 1.26^{+0.06}_{-0.12}$. This provides an acceptable fit, with $\chi^2_{\rm r}$/dof = 0.96/405 (Figure 4). The improvement of the chi-squared statistic is significant at more than the 99.9% confidence level when compared to the single power-law model. Next, we considered an alternative fit consisting of a power-law function and a blackbody component. This model also gives a good representation of the data, with $\chi^2_{\rm r}$ of 0.97 for 405 dof, indicating that the photon index is $\Gamma = 1.32 \pm 0.03$ and the temperature of the introduced thermal component is $kT = 0.15 \pm 0.03$ keV. This result is consistent with previous *Suzaku* ($\Gamma = 1.24 \pm 0.01$; Kataoka et al. 2008) and BeppoSAX observations ($\Gamma = 1.39 \pm 0.08$; Tavecchio et al. 2000).

*3C 454.3.* We first fitted the XISs and PIN spectra with a single power-law model with a Galactic absorption of $N_{\rm H} = 7.24 \times 10^{20}$ cm$^{-2}$ (Murphy et al. 1996). We obtained the photon index of $\Gamma = 1.58 \pm 0.01$ ($\chi^2_{\rm r} = 1.00$ for 1090 dof), but the residuals show some scatter around 1 keV (Figure 2). To investigate this scatter in more detail, we fitted the spectra with a single power-law and a free absorption model. This model represents well the spectra with the best chi-squared value of 0.97 for 1089 dof, indicating that the column density is higher than the Galactic value at the 99.9% confidence level. For this model the photon index is $\Gamma = 1.62 \pm 0.01$ and a column density of $N_{\rm H} = (9.07^{+0.58}_{-0.57}) \times 10^{20}$ cm$^{-2}$. The unabsorbed 2–10 keV flux is $F_{2-10\,\rm keV} = (1.66 \pm 0.02) \times 10^{-11}$ erg cm$^{-2}$ s$^{-1}$ (Figure 3). The spectra can be fitted with both the Galactic absorption and a broken power-law model as well as the above model ($\chi^2_{\rm r}$/dof of 0.96/1088). In the former case, the photon indices are $\Gamma_1 = 1.47^{+0.04}_{-0.05}$ and $\Gamma_2 = 1.61 \pm 0.01$, while the break energy is $E_{\rm brk} = 1.29^{+0.14}_{-0.16}$ keV. In addition, we reanalyzed the previous *Suzaku* data collected in 2007 December during the high state (Donnarumma et al. 2009). The time-averaged XISs and HXD/PIN spectra was well described by a single absorbed power-law model with $\Gamma = 1.64 \pm 0.01$, implying the flux $F_{2-10\,\rm keV} = (3.11 \pm 0.03) \times 10^{-11}$ erg cm$^{-2}$ s$^{-1}$, which

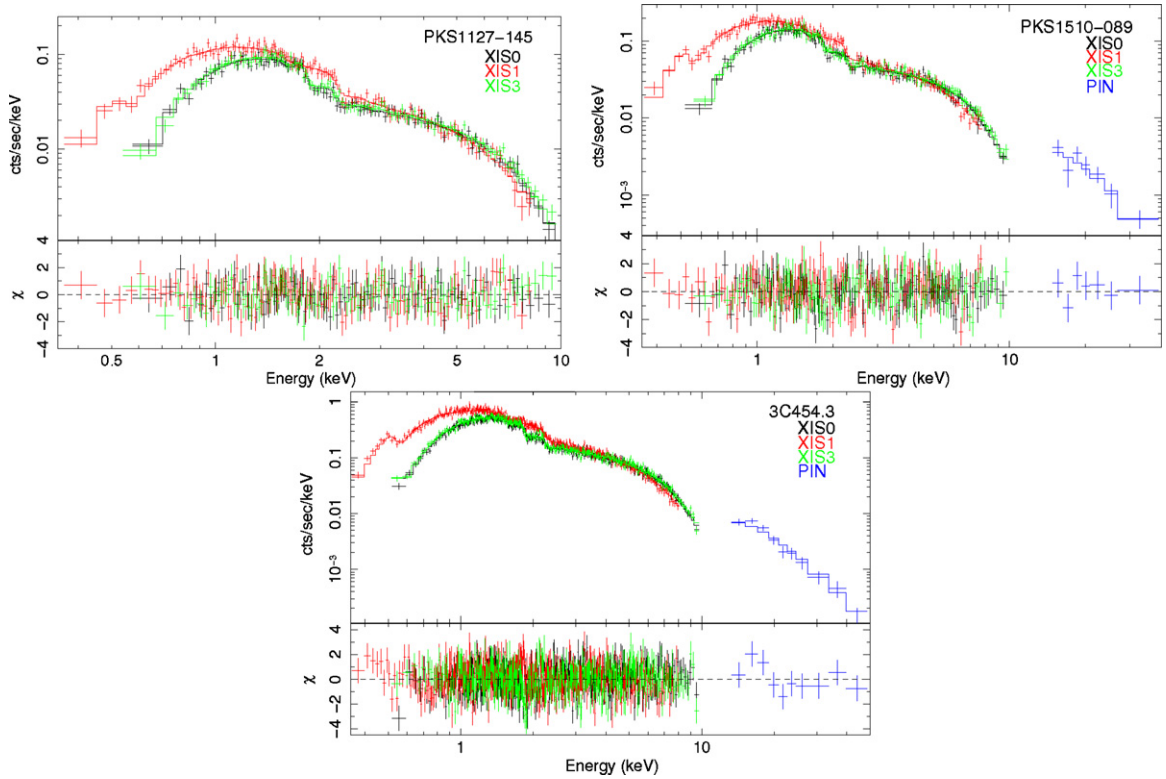


**Figure 4.** Best-fit *Suzaku* spectrum of PKS 1127−145, PKS 1510−089, and 3C454.3. The top panel shows the data, plotted against an absorbed power-law model. The bottom panel shows the residuals to the power-law fit.

(A color version of this figure is available in the online journal.)

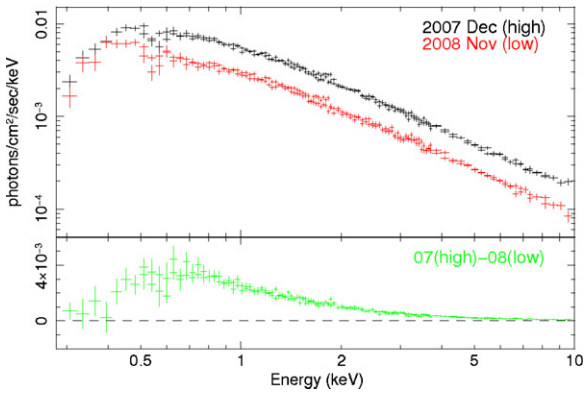


**Figure 5.** Unfolded spectra of 3C 454.3 obtained in 2007 (high) and 2008 (low), respectively. The bottom panel shows the residuals by subtracting the spectra in the high state from those in the low state.

(A color version of this figure is available in the online journal.)

is larger by a factor of 2 than the one found in our 2008 observations. The absorption column also shows a higher value of $N_{\rm H} = (1.07 \pm 0.04) \times 10^{21}$ cm$^{-2}$.

Figure 5 shows the unfolded spectra obtained in 2007 (high state) and 2008 (this work; low state). The bottom panel shows the residuals by subtracting the spectra in the high state from those in the low state. The excess emission at low energies is clearly visible in the residuals.

The previous X-ray observations of 3C 454.3 often indicated some additional absorption in excess to the Galactic value. For example, Villata et al. (2006) reported $N_{\rm H} = (1.34 \pm 0.05) \times 10^{21}$ cm$^{-2}$ in the *Chandra* data collected in 2005 May, during the outburst phase ($F_{2-8\,\rm keV} \sim 8.4 \times 10^{-11}$ erg cm$^{-2}$ s$^{-1}$, which is ∼5 times higher than in our observation). An even higher hydrogen column density was found by Giommi et al. (2006), when fitting the 2005 April–May data taken by the *Swift* XRT ($N_{\rm H} \sim 2$–$3 \times 10^{21}$ cm$^{-2}$), and by Raiteri et al. (2007, 2008), using the 2006 July and December, and 2007 May data taken by *XMM-Newton*. Assuming that the intrinsic absorption in 3C 454.3 is the same as reported in Villata et al. (2006), we fit our *Suzaku* data first by a double power-law function, obtaining $\Gamma_1 = 3.66^{+0.60}_{-0.53}$ and $\Gamma_2 = 1.61 \pm 0.03$. This provides an acceptable fit, with $\chi^2_{\rm r}/{\rm dof} = 0.97/1088$. Next we consider an alternative fit consisting of a power-law and a blackbody component. This model gives a good representation of the data, with $\chi^2_{\rm r}/{\rm dof} = 1.00/1088$, a photon index of $\Gamma = 1.65 \pm 0.01$, and a temperature of $kT = 0.105^{+0.007}_{-0.009}$ keV. However, the fitting results do not improve the goodness of fit compared with the single power-law model with free absorption.

#### 3.1.3. Time-resolved Spectral Analysis

In order to investigate the X-ray spectral evolution of each object, we divided the total exposure into one-orbit intervals (∼5760 s). We fitted the overall XIS spectra between 0.3 and 10 keV with an absorbed simple power-law function. The photoelectric absorbing column densities were fixed at the values derived in Section 3.1.2. Figure 6 shows the relation between the 2–10 keV fluxes versus the photon indices measured by the *Suzaku* XISs. Significant spectral variation is seen in PKS 0208−512 ($\Gamma = 1.4$–$1.8$), Q 0827+243 ($\Gamma = 1.2$–$1.6$), PKS 1127−145 ($\Gamma = 1.4$–$1.6$), and PKS 1510−089 ($\Gamma = 1.3$–$1.5$). In the case of 3C 454.3, the X-ray photon index is only weakly variable around the mean value $\Gamma \sim 1.6$. Figure 6 clearly reveals a spectral evolution with the X-ray spectra hardening as the sources become brighter. Such a trend is often observed in high-frequency-peaked BL Lac objects (e.g., Kataoka et al. 1999), but it has never been observed so clearly in FSRQs (but see Kataoka et al. 2008 for PKS 1510−089).

**Table 5**
Results of the Spectral Fits to the *Swift* XRT Data Using a Power Law with Galactic Absorption

| Object | $N_{\rm H}$[a] | $\Gamma$ | $F_{2-10\,\rm keV}$[b] | $\chi^2_{\rm r}$ (dof) |
|---|---|---|---|---|
| 0208−512 | 3.08 (fixed) | 1.96 ± 0.24 | 1.37 ± 0.06 | 0.33 (13) |
| 0827+243 | 3.62 (fixed) | 1.46 ± 0.35 | $1.13^{+0.55}_{-0.43}$ | 1.12 (8) |
| 1127−145 | 3.83 (fixed) | 1.28 ± 0.03 | 6.14 ± 0.23 | 1.28 (94) |
| 1510−089 | 7.88 (fixed) | 1.38 ± 0.08 | $6.09^{+0.65}_{-0.62}$ | 0.71 (31) |
| 3C 454.3 | 7.24 (fixed) | 1.53 ± 0.09 | 17.6 ± 2.1 | 1.41 (18) |

**Notes.** Errors correspond to 1$\sigma$ confidence level.

[a] Fixed value indicates the Galactic absorption column density in units of $10^{20}$ cm$^{-2}$.

[b] Flux in units of $10^{-12}$ erg cm$^{-2}$ s$^{-1}$.

### 3.2. Swift

Since the effective area of the *Swift* XRT is less than 10% of the *Suzaku* XIS in the 0.5–10 keV range, detailed spectral modeling is difficult using *Swift* data. Furthermore, the average exposure for the *Swift* observation was only a few kiloseconds, which was much less than the *Suzaku* exposure. We therefore fit the XRT data simply with a power-law model with Galactic absorption in the energy range 0.3–10 keV for the cross-calibration between the two instruments. The results of the spectral fits are summarized in Table 5. We can see that the results obtained with *Suzaku* and *Swift* are consistent within the range of error except PKS 1127−145.

The UVOT fluxes in each filter were corrected for Galactic extinction following the procedure described in Cardelli et al. (1989). We generated a list of the amount of extinction that needs to be accounted for in each filter, $A_\lambda = E_{B-V}(aR_V + b)$, where $a$ and $b$ are constants. The Cardelli procedure provides a good approximation to the UV-through-IR Galactic dust extinction as a function of the total-to-selective extinction, $R_V$, which throughout this paper we assume to be $R_V = 3.1$, which is the mean Galactic value. The observed magnitudes and correction factors for each of the filters are summarized in Tables 6 and 7, respectively.

### 3.3. Fermi LAT

To study the average spectra of five objects during the four or five months of observations, we use the standard maximum-likelihood spectral estimator provided with the LAT science tools GTLIKE. This fits the data to a source model, along with models for the uniform extragalactic and structured Galactic backgrounds. Photons were extracted from a region with a 10° radius centered on the coordinates of the position of each object. The Galactic diffuse background model is the currently recommended version (gll_iem_v02[66]), with the normalization free to vary in the fit. The response function used is P6_V3_DIFFUSE.

For simplicity, we model the continuum emission from each source with a single power law. It is likely that such a model might be too simple, as shown in the paper reporting spectra of

[66] This model is available for download from the Fermi Science Support Center, http://fermi.gsfc.nasa.gov/ssc.

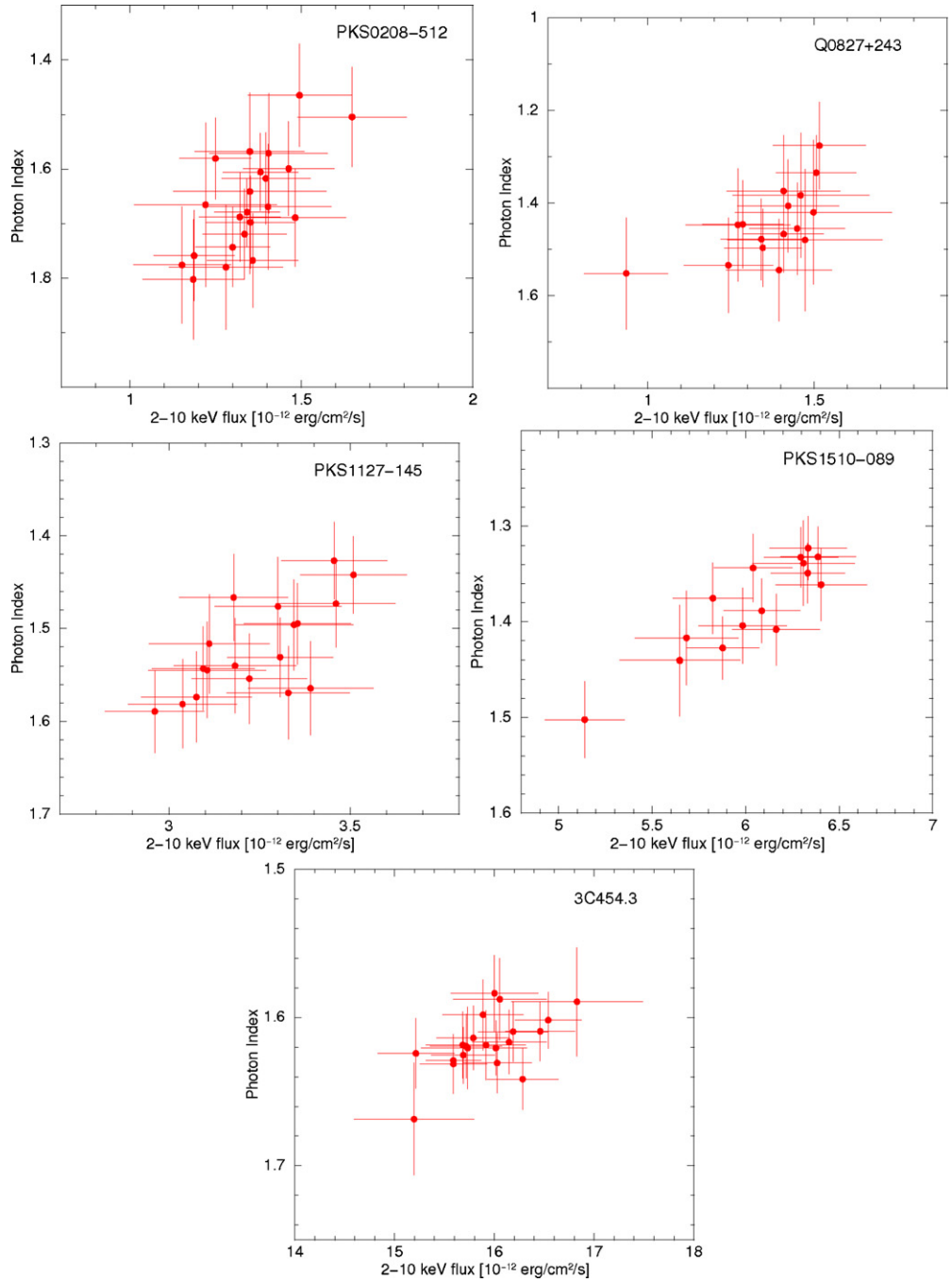


**Figure 6.** Correlation of the 2–10 keV flux vs. photon index of five blazars as measured by the *Suzaku* XISs.
(A color version of this figure is available in the online journal.)

**Table 6**
*Swift* UVOT Magnitudes of Five FSRQs

| Object | $v$ (mag) | $b$ (mag) | $u$ (mag) | uvw1 (mag) | uvm2 (mag) | uvw2 (mag) | $E(B-V)$ |
|---|---|---|---|---|---|---|---|
| 0208−512 | $17.64^{+0.14}_{-0.12}$ | $17.94^{+0.09}_{-0.08}$ | $17.17^{+0.09}_{-0.08}$ | 16.84 ± 0.07 | 16.71 ± 0.07 | $17.00^{+0.06}_{-0.05}$ | 0.022 |
| 0827+243 | ... | ... | 16.57 ± 0.01 | ... | ... | ... | 0.033 |
| 1127−145 | 16.48 ± 0.02 | 16.70 ± 0.01 | 15.64 ± 0.01 | 15.51 ± 0.01 | 15.56 ± 0.01 | 15.79 ± 0.01 | 0.037 |
| 1510−089 | ... | ... | 16.01 ± 0.02 | 16.27 ± 0.02 | 16.13 ± 0.02 | ... | 0.097 |
| 3C 454.3 | $16.05^{+0.09}_{-0.08}$ | 16.52 ± 0.06 | 15.72 ± 0.06 | 15.75 ± 0.06 | 15.81 ± 0.08 | 16.06 ± 0.05 | 0.107 |

**Notes.** Observed magnitude for each observation using specific filter (Galactic extinction not corrected).

**Table 7**
Correction Factors for the Galactic Extinction in UV and Optical Filters

| Param | | *v* | *b* | *u* | uvw1 | uvm2 | uvw2 |
|---|---|---|---|---|---|---|---|
| $\lambda^a$ | (nm) | 547 | 439 | 346 | 260 | 249 | 193 |
| $a^b$ | | 1.0015 | 0.9994 | 0.9226 | 0.4346 | 0.3494 | −0.0581 |
| $b^b$ | | 0.0126 | 1.0171 | 2.1019 | 5.3286 | 6.1427 | 8.4402 |
| | 0208−512 | 0.07 | 0.09 | 0.11 | 0.15 | 0.16 | 0.18 |
| | 0827+243 | ... | ... | 0.16 | ... | ... | ... |
| $A_\lambda{}^b$ | 1127−145 | 0.12 | 0.15 | 0.18 | 0.25 | 0.27 | 0.31 |
| | 1510−089 | ... | ... | 0.48 | 0.65 | 0.70 | ... |
| | 3C 454.3 | 0.33 | 0.44 | 0.53 | 0.71 | 0.77 | 0.88 |

**Notes.**
[a] Center wavelength for each optical and UV filter.
[b] Parameters for calculating Galactic extinction for optical and UV filters, calculated according to the prescription in Cardelli et al. (1989). The Galactic reddening was taken from f et al. (1998).

**Table 8**
Results of the Spectral Fits to the *Fermi* LAT Data

| Object | Γ | $F_{>100\,\mathrm{MeV}}{}^a$ | TS[b] |
|---|---|---|---|
| 0208−512 | 2.33 ± 0.05 | 0.26 ± 0.03 | 1484 |
| 0827+243 | 2.62 ± 0.36 | 0.05 ± 0.04 | 58 |
| 1127−145 | 2.75 ± 0.14 | 0.15 ± 0.04 | 234 |
| 1510−089 | 2.48 ± 0.03 | 0.69 ± 0.04 | 4224 |
| 3C 454.3 | 2.50 ± 0.02 | 2.55 ± 0.08 | 25144 |
| 1510−089[c] | 2.28 ± 0.27 | 0.91 ± 0.51 | 59 |
| 3C 454.3[c] | 2.62 ± 0.13 | 2.59 ± 0.58 | 281 |

**Notes.**
[a] Flux in units of $10^{-6}$ ph cm$^{-2}$ s$^{-1}$.
[b] Test statistic: defined as TS = $2(\log L - \log L_0)$, where $L$ and $L_0$ are the likelihood when the source is included or not.
[c] Corresponding data collected during the *Suzaku* observing period.

bright Fermi blazars (Abdo et al. 2010), where the gamma-ray data suggest a steepening of the spectrum with energy, well-described as a broken power law. However, here, we are reporting cases of blazars in low-level activity states and thus relatively faint, where fits to a broken power-law model would result in poorly constrained spectral parameters for a more complex model; furthermore, we note that the use of such a more complex spectral model in the gamma-ray band does not alter our conclusions or significantly change the parameters in Table 10. The extragalactic background is assumed to have a power-law spectrum, with its spectral index and the normalization free to vary in the fit. From an unbinned GTLIKE fit the best-fit photon indices are $\Gamma = 2.33 \pm 0.05$ for PKS 0208−512, $\Gamma = 2.62 \pm 0.35$ for Q 0827+243, $\Gamma = 2.77 \pm 0.14$ for PKS 1127−145, $\Gamma = 2.48 \pm 0.03$ for PKS 1510−089, and $\Gamma = 2.51 \pm 0.02$ for 3C 454.3 (see also Table 8). Here only statistical errors are taken into account, and we report fluxes using spectra extrapolated down to 100 MeV. In the case of bright sources (PKS 1510−089 and 3C 454.3), we also analyzed the data collected during the *Suzaku* observing period to construct the simultaneous broadband spectra spectra.

Table 9 summarizes the flux in seven energy bands obtained by separately running GTLIKE for each energy band: 200–400 keV, 400–800 keV, 800–1600 keV, 1600–3200 keV, 3200–6400 keV, 6400–12800 keV, 12800–25600 keV, respectively.

## 4. DISCUSSION

### *4.1. Broadband Spectra Spectral Fits*

We constructed the broadband SED ranging from the radio to $\gamma$-ray bands for the five observed FSRQs, and these are shown in Figure 7. Here the filled red circles and solid lines represent simultaneous data from the UV/optical (*Swift* UVOT), X-ray (*Suzaku*), and $\gamma$-ray (*Fermi* LAT) observations. Quasi-simultaneous data are also shown as red open triangles and dashed lines. Historical radio (NED) and $\gamma$-ray (EGRET) data are also plotted as filled blue circles. Green symbols in the SEDs of PKS 1510−089 and 3C 454.3 denote the previous simultaneous observations (Kataoka et al. 2008; Donnarumma et al. 2009).

In order to model the constructed SEDs, we applied the synchrotron-IC emission model described in Tavecchio & Ghisellini (2008), where both synchrotron and external (BLR and DT) photons are considered as seed radiation fields contributing to the IC process (SSC+ECR). The electron distribution is modeled as a smoothly broken power law

$$N'(\gamma) = K\,\gamma^{-n_1}\left(1+\frac{\gamma}{\gamma_{\rm br}}\right)^{n_1-n_2}, \quad (1)$$

where $K$ (cm$^{-3}$) is a normalization factor, $n_1$ and $n_2$, are the energy indices below and above the break Lorentz factor $\gamma_{\rm br}$. The electron distribution extends within the limits $\gamma_{\rm min} < \gamma < \gamma_{\rm max}$. We also assume that the "blazar emission zone," with the comoving size $R$ and magnetic field intensity $B$, is located at the distance $r$ such that $r_0 < r < r_{\rm BLR} < r_{\rm DT}$, where $r_0$ is the distance below which the photon energy density in the jet rest frame is dominated by the direct radiation of the accretion disk, $r_{\rm BLR}$ is the characteristic scale of the BLR, and $r_{\rm DT}$ is the scale of the DT (see the discussion in Tavecchio & Ghisellini 2008 as well as in Sikora et al. 2009). This choice, while somewhat arbitrary, has been validated by a number of authors modeling broadband spectra of FSRQs. Hence, the comoving energy density of the dominant photon field—provided by the BLR—is

$$U'_{\rm rad} \simeq \Gamma_j^2\,\frac{\eta_{\rm BLR} L_{\rm d}}{4\pi r_{\rm BLR}^2 c}, \quad (2)$$

where $\Gamma_j$ is the jet bulk Lorentz factor, and the BLR is assumed to reprocess $\eta_{\rm BLR} \simeq 10\%$ of the disk luminosity $L_{\rm d}$. Finally, we assume that the jet viewing angle is in all the cases $\theta_j \simeq 1/\Gamma_j$, so that the jet Doppler factor $\delta_j \simeq \Gamma_j$.

The results of model fitting are shown in different panels of Figure 7, and the resulting parameters are summarized in Table 10. In the context of this model, where we assume the dissipation region to be between the immediate vicinity of the accretion disk but within the BLR, it is clear that in all cases the LAT fluxes are dominated by the IC/BLR component, while in the X-ray band both IC/BLR and IC/DT processes may contribute at a comparable level. In addition, the SSC emission seems negligible, being in particular too weak to account for the soft X-ray excess discussed in the previous sections. This excess, on the other hand, may be well represented by the high-energy tail of the synchrotron continuum, or an additional blackbody-type spectral component.

Based on the model results, for each object we compute the ratio of the comoving energy densities stored in jet electrons and the magnetic field,

$$\frac{U'_e}{U'_B} = \frac{\int_{\gamma_{\rm min}}^{\gamma_{\rm max}} \gamma\, m_e c^2\, N'(\gamma)\, d\gamma}{B^2/8\pi}, \quad (3)$$

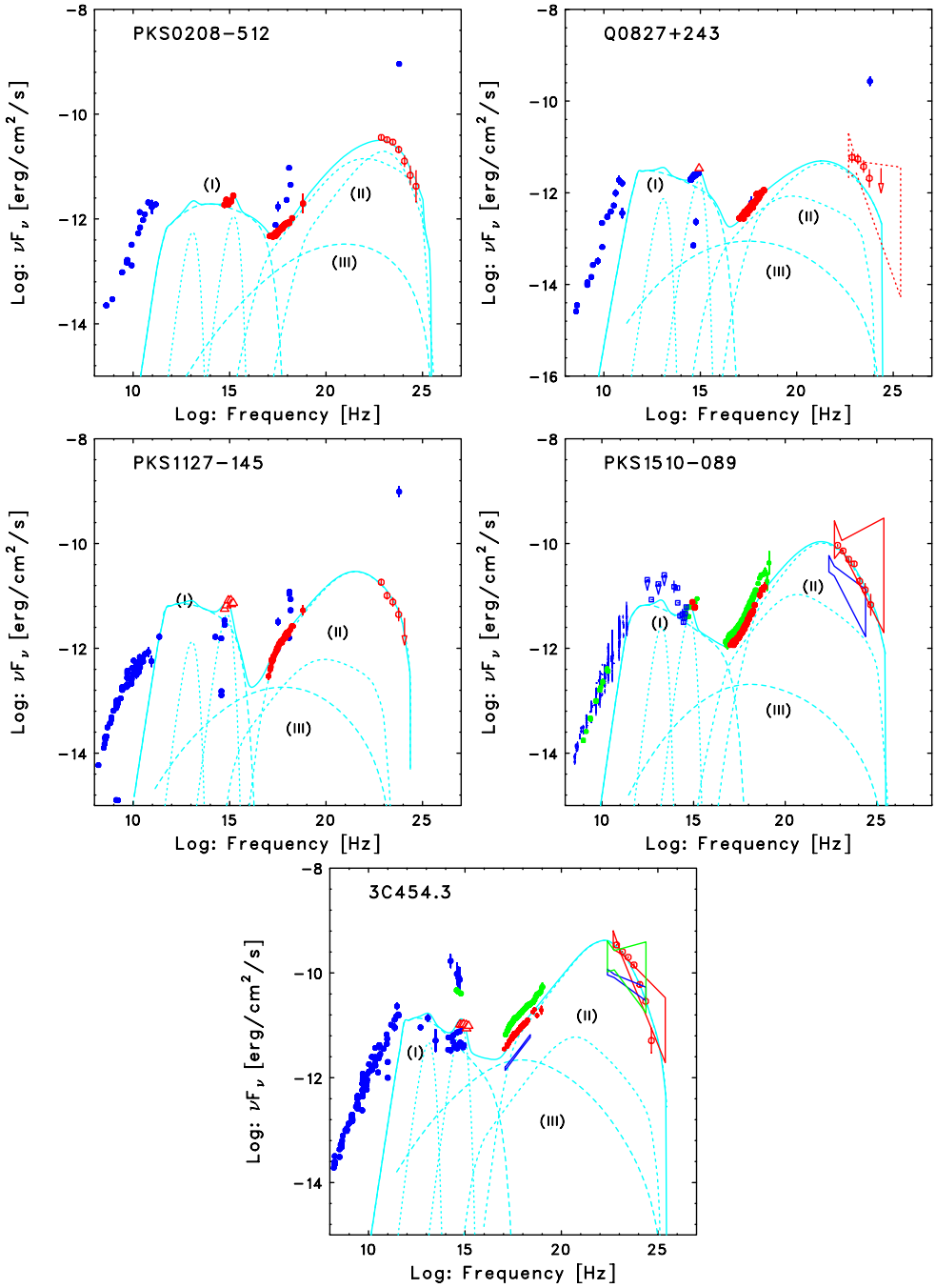


**Figure 7.** Overall SED of five sources constructed with broadband data obtained during 2008 October to 2009 January (filled red circles and solid bow-tie). Quasi simultaneous data are also shown (open red circles). Historical radio (NED) and $\gamma$-ray (EGRET) data are also plotted as filled blue circles. Green symbols in the SEDs of PKS 1510−089 and 3C 454.3 denote the previous simultaneous observations (Kataoka et al. 2008; Donnarumma et al. 2009). The dotted lines show (I) the synchrotron and (II) the EC components, and (III) SSC components, respectively. The solid line shows the jet continuum calculated with the jet emission model described in Section 4.2.

**Table 9**
Results of *Fermi* LAT Data Analysis from 200 MeV to 25600 MeV (Flux in Units of $10^{-9}$ ph MeV$^{-1}$ cm$^{-2}$ s$^{-1}$)

| Object | Band 1[a] | Band 2[a] | Band 3[a] | Band 4[a] | Band 5[a] | Band 6[a] | Band 7[a] |
|---|---|---|---|---|---|---|---|
| 0208−512 | 3.24 ± 0.25 | 3.69 ± 0.30 | 4.19 ± 0.42 | 3.81 ± 0.61 | 2.88 ± 0.79 | 1.95 ± 1.00 | 1.51 ± 1.49 |
| 0827+243 | 0.73 ± 0.22 | 1.03 ± 0.28 | 1.08 ± 0.36 | 0.92 ± 0.50 | ... | ... | ... |
| 1127−145 | 2.65 ± 0.34 | 2.50 ± 0.43 | 3.21 ± 0.68 | 3.17 ± 1.05 | ... | ... | ... |
| 1510−089 | 9.74 ± 0.38 | 10.62 ± 0.48 | 10.19 ± 0.67 | 11.57 ± 1.09 | 7.51 ± 1.47 | 7.15 ± 2.26 | 5.14 ± 3.01 |
| 3C 454.3 | 37.22 ± 0.67 | 39.36 ± 0.91 | 43.79 ± 1.42 | 44.20 ± 2.31 | 26.65 ± 2.96 | 17.98 ± 3.99 | 4.55 ± 3.28 |

**Notes.**
[a] Band 1: 200–400 MeV, Band 2: 400–800 MeV, Band 3: 800–1600 MeV, Band 4: 1600–3200 MeV, Band 5: 3200–6400 MeV, Band 6: 6400–12800 MeV, and Band 7: 12800–25600 MeV.

**Table 10**
Model Parameters Used to Calculate the SEDs of Five FSRQs

| Object | $n_1$ | $n_2$ | $\gamma_{\rm min}$ | $\gamma_{\rm br}$ | $\gamma_{\rm max}$ | $K$ ($10^4$ cm$^{-3}$) | $\Gamma_j$ | $R$ ($10^{16}$ cm) | $B$ (G) | $L_{\rm d}$ ($10^{46}$ erg s$^{-1}$) | $r_{\rm BLR}$ ($10^{18}$ cm) | $r_{\rm DT}$ ($10^{18}$ cm) |
|---|---|---|---|---|---|---|---|---|---|---|---|---|
| 0208−512 | 2 | 3.3 | 3.0 | 700 | $4.3 \times 10^4$ | 2.2 | 15 | 1.8 | 1.1 | 1.5 | 0.76 | 3.0 |
| 0827+243 | 2 | 3.3 | 1.5 | 300 | $1.0 \times 10^4$ | 8.5 | 10 | 1.8 | 3.8 | 2.0 | 1.3 | 4.2 |
| 1127−145 | 2 | 3.4 | 1.2 | 110 | $5.0 \times 10^3$ | 0.65 | 10 | 6.5 | 4.1 | 10 | 0.8 | 10 |
| 1510−089 | 2 | 3.5 | 3.0 | 190 | $4.6 \times 10^4$ | 0.81 | 13 | 4 | 0.8 | 0.3 | 0.48 | 4 |
| 3C 454.3 | 2 | 3.8 | 1.0 | 290 | $3.0 \times 10^4$ | 4.5 | 12 | 3.2 | 0.8 | 4.0 | 1.5 | 30 |

**Table 11**
Jet Parameters of Five FSRQs in Low-activity States

| Object | $U'_e/U'_B$ | $L_j$ ($10^{46}$ erg s$^{-1}$) | $\eta_j$ | $\langle\gamma\rangle$ |
|---|---|---|---|---|
| 0208−512 | 2 | 0.8 | 0.06 | 16 |
| 0827+243 | 0.6 | 2.8 | 0.14 | 8 |
| 1127−145 | 0.03 | 5.8 | 0.06 | 5 |
| 1510−089 | 0.9 | 1 | 0.35 | 12 |
| 3C 454.3 | 7 | 9.4 | 0.23 | 5 |

where $B$ is the magnetic field intensity in the emission region. In addition, we compute the implied total kinetic jet power as

$$L_j = \pi R^2 c \Gamma_j^2 (U'_e + U'_B + U'_p), \quad (4)$$

where $R$ is the emission region linear size, and $U'_p$ is the energy density of cold protons. The latter parameter is estimated assuming one proton per ten electron–positron pairs (see the discussion in Sikora et al. 2009), namely $U'_p = 0.1\, m_p c^2 \int_{\gamma_{\rm min}}^{\gamma_{\rm max}} N'(\gamma)\, d\gamma$. The resulting total kinetic power of the outflow is then compared with the accretion luminosity (assuming standard accretion disk with 10% radiative efficiency), by means of the evaluated efficiency parameter $\eta_j = L_j/L_{\rm acc} \simeq L_j/10\, L_{\rm d}$, where $L_{\rm d}$ is the disk luminosity implied by the model fitting (see Table 10). Note that with the above model assumptions and the model parameters inferred by us, the jets of objects considered here are dynamically dominated by cold protons, $U'_p/U'_e \simeq 200/\langle\gamma\rangle > 1$, since the mean Lorentz factor of the radiating ultra-relativistic electrons is in all the cases $\langle\gamma\rangle \ll 200$ (see Table 11).

Some of the derived jet parameters for five luminous blazars in their low-activity states are significantly different from the analogous parameters claimed for the flaring states, *even in the same object*. For example, in the case of the high-activity state of PKS 1510−089, Kataoka et al. (2008) estimated (under the same assumptions regarding the jet content as in this paper) the total kinetic power of the jet as $L_j \sim 2.7 \times 10^{46}$ erg s$^{-1}$, which is larger than the value derived in this paper, by about a factor of 3. In addition, our model values of the jet bulk Lorentz factors are also systematically lower than the ones given in the literature ($\Gamma_j \simeq 10$ versus 20). Interestingly, other jet parameters, such as magnetic field intensity, $B \simeq 1$ G, and the equipartition ratio, $U'_e/U'_B \sim 1$, or the general spectral shape of the electron energy distribution, are comparable to the ones found for flaring FSRQs, (albeit with a substantial scatter). It should be noted in this context, however, that for the three sources considered in this paper (namely PKS 1127−145, PKS 1510−089, and 3C 454.3), the flaring states were analyzed in a framework of the IC/DT model (Błażejowski et al. 2004; Kataoka et al. 2008; Sikora et al. 2008, respectively), while here, we argue that the IC/BLR contribution is dominant, as motivated by the detected relatively short (day) variability timescale of the X-ray continua. On the other hand, as discussed recently in Sikora et al. (2009), there is a so-called "conspiracy" between the IC/BLR and IC/DT models, in a sense that the resulting inferred jet parameters are comparable in both cases. Hence, we can safely conclude that the low- and high-activity states of luminous blazar sources are due to the low and high total kinetic power of the jet, respectively, possibly related to varying bulk Lorentz factors within the blazar emission zone. And indeed, keeping in mind that the highly dynamical and complex jet formation processes in the closest vicinity of supermassive black holes—most likely shaped by accretion process subjected to several possible instability of the jet fuel, especially when the accretion rate is close to Eddington—such a significant variation in the total kinetic output of the outflow should not be surprising. Further support for this scenario comes from the fact that the jet efficiency factors estimated here, $\eta_j \lesssim 1$, are significantly lower than the ones found for powerful blazars in their flaring states (see Sambruna et al. 2006; Ghisellini et al. 2009), even if the difference in the jet proton content adopted by various authors is taken into account.

### 4.2. Spectral Evolution

As shown in Section 3.1.3, the X-ray spectra of the FSRQs analyzed here flatten with increasing flux. For $\Gamma_{\rm j} \sim \delta_{\rm j} \sim 10$ and the dominant IC/BLR emission process, the electrons emitting the observed 1–10 keV photons have Lorentz factor $\gamma \sim \gamma_{\rm min} \sim$ few. The electrons emitting X-ray photons in these sources are very low energy, so cooling effects cannot play any role in the observed spectral evolution. In particular, it can be easily demonstrated that in a framework of our model (i.e., for the dominant IC/BLR energy losses), a strong cooling regime is expected only for the electrons with Lorentz factors greater than

$$\gamma_{\rm cr} \simeq \frac{3\pi\, m_e c^3\, r_{\rm BLR}^2}{\sigma_{\rm T}\, R\, \Gamma_j^2\, \eta_{\rm BLR} L_{\rm d}} \simeq 350 \left(\frac{r_{\rm BLR}}{10^{18}\,{\rm cm}}\right)^2 \left(\frac{\eta_{\rm BLR}}{0.1}\right)^{-1} \left(\frac{\Gamma_j}{10}\right)^{-2} \left(\frac{L_{\rm d}}{10^{46}\,{\rm erg\,s^{-1}}}\right)^{-1} \times \left(\frac{R}{10^{16}\,{\rm cm}}\right)^{-1}. \quad (5)$$

This, for the fitting parameters as given in Table 10, is typically above or just around the break Lorentz factor, $\gamma_{\rm cr} \gtrsim \gamma_{\rm br}$ (in agreement with the discussion in Sikora et al. 2009). Adiabatic losses, if present, should not result in changing the slope of the power-law X-ray continua as well. Thus, one may suspect that the revealed spectral changes are shaped by the acceleration process within the blazar emission zone. In the case of relativistic jets the relevant acceleration processes are still quite uncertain, although, as pointed out by Kataoka et al. (2008) and Sikora et al (2009), the repeatedly observed flat X-ray photon indices $\Gamma \leqslant 1.5$ seem to favor the mechanism

discussed by Hoshino et al. (1992) for the low-energy segment of the electron energy distribution. In this model, the low-energy electrons (with Lorentz factors, roughly, $\gamma < m_p/m_e$) are accelerated by a resonant absorption of the cyclotron emission generated by cold protons reflected from the shock front. As shown later by Amato & Arons (2006), the power-law slope of these accelerated electrons depends on the relative number of electrons to protons at the shock front. Hence, a larger fraction of the energy carried by jet protons during the higher-activity states should in principle result in a more efficient acceleration of jet electrons and their flatter spectrum, in agreement with the observed X-ray spectral evolution discussed here.

The above interpretation, on the other hand, would imply a significant variability in the $\gamma$-ray frequency range. Indeed, the broken power-law form of the electron energy distribution revealed by our spectral modeling discussed in the previous section implies the $\gamma$-ray flux $F_\gamma \equiv [\nu F_\nu]_\gamma$ around the IC spectral peak $\nu_\gamma \sim 10^{22}$ Hz should be, roughly

$$F_\gamma \simeq F_X \left(\frac{\nu_\gamma}{\nu_X}\right)^{2-\Gamma} \simeq 10^{4\,(2-\Gamma)} F_X\,, \qquad (6)$$

where $F_X$ is the monochromatic X-ray flux measured around $\nu_X \sim 10^{18}$ Hz, and $\Gamma$ is the observed X-ray photon index. For example, our analysis for PKS 0208−512 indicates a photon index $\Gamma_1 \sim 1.8$ for an X-ray flux $F_{X,1} \sim 1.2 \times 10^{-12}$ erg cm$^{-2}$ s$^{-1}$ in the lower state, and $\Gamma_2 \sim 1.5$ for $F_{X,2} \sim 1.6 \times 10^{-12}$ erg cm$^{-2}$ s$^{-1}$ in the higher state. Thus, if the observed X-ray variability is due to flattening of the electron energy distribution during the acceleration process, one should observe the $\gamma$-ray variability of the order of

$$\frac{F_{\gamma,2}}{F_{\gamma,1}} \simeq 10^{4\,(\Gamma_1-\Gamma_2)}\,\frac{F_{X,2}}{F_{X,1}} \sim 20\,. \qquad (7)$$

However, during the simultaneous *Fermi* observation, no significant $\gamma$-ray variability was observed for the analyzed sources, at least within one day timescale.

Therefore, the most viable explanation for the observed X-ray spectral evolution is that the IC power-law slope remains roughly constant during the flux variations, but the amount of contamination from the additional soft X-ray component increases at low flux levels, affecting the spectral fitting parameters at higher photon energies ($> 2$ keV). Note that in such a case the expected gamma-ray variability should be of the same order as the X-ray variability, namely $F_{\gamma,2}/F_{\gamma,1} \simeq F_{X,2}/F_{X,1} \sim 1.3$.

We finally note in this context that, as shown in Section 3.1.2, the previous BeppoSAX data for PKS 0208−512 collected during the high state indicated a convex X-ray spectrum, and an excess absorption below 1 keV with a column density of $N_{\rm H} \sim 1.67 \times 10^{21}$ cm$^{-2}$ exceeding the Galactic value by more than a factor of 5. However, the X-ray photon index was similar to the one implied by our *Suzaku* observations ($\Gamma \sim 1.7$). Therefore, the convex spectrum observed by BeppoSAX may reflect an intrinsic shape of the IC emission involving the low-energy cutoff in the electron energy distribution around $\gamma \sim 1$, as expected in the EC/BLR model (Tavecchio et al. 2007), which is only diluted during the low-activity states due to the presence of an additional soft X-ray spectral component.

A similar trend has been observed in 3C 454.3. To illustrate this, in Figure 8 we selected the data which have a similar power-law slope ($\Gamma \sim 1.6$) and plotted the absorption column versus 2–10 keV flux densities derived from the *Chandra* (Villata et al. 2006), *Swift* (Giommi et al. 2006), *XMM-Newton* (Raiteri et al. 2007, 2008), and *Suzaku* (this work) observations. We can see that there is a trend of increasing the absorption value with source brightness, as previously reported by Raiteri et al. (2007, 2008). These results may again be explained by the soft excess emission being more important when the source gets fainter, and becoming almost completely "hidden" behind the hard X-ray power law when the source gets brighter.

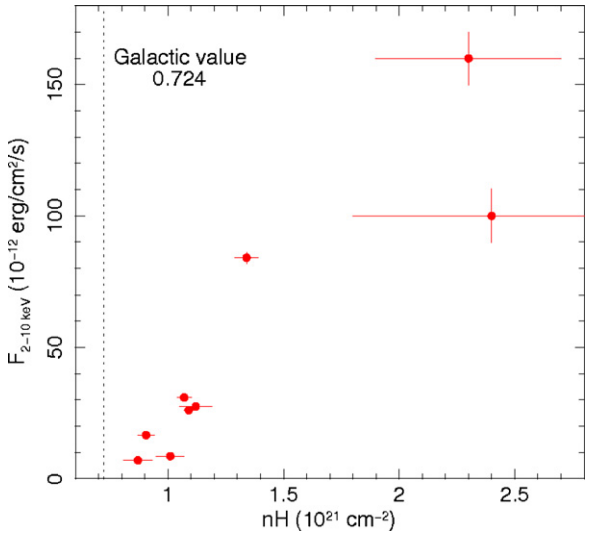


**Figure 8.** Fluxes in the 2–10 keV band for different observations of 3C 454.3 vs. $N_{\rm H}$ for the fits with an absorbed power-law model. The dashed line indicates the Galactic absorption column. This figure indicates that the intrinsic X-ray spectrum is not a simple power law, but instead, it shows some curvature, which may depend on the X-ray brightness.

(A color version of this figure is available in the online journal.)

From the spectral fitting of the *Suzaku* data, we showed in Section 3.1.2 that the soft X-ray excess may be represented either by a steep power-law ($\Gamma \sim 3$–5) or a blackbody-type emission ($kT \sim 0.1$–0.2 keV). Since the synchrotron peak of each source is located around optical photon energies (see Figure 7), the high-energy synchrotron tail may possibly account for the observed soft X-ray excess emission, especially if being modified by the Klein-Nishina effects (see the discussion in Sikora et al. 2009; Kataoka et al. 2008). On the other hand, the bulk-Compton spectral component produced by Comptonization of the UV accretion disk by cold electrons in the innermost parts of relativistic jets (e.g., Begelman & Sikora 1987) is a natural explanation for the apparent soft X-ray excess component.

## 5. CONCLUSIONS

We have presented the observations and analysis of the data for the $\gamma$-ray-loud blazars, PKS 0208−512, Q 0827+243, PKS 1127−145, PKS 1510−089, and 3C 454.3, obtained with the *Suzaku*, *Swift* UVOT, and *Fermi* LAT. Observations were conducted between 2008 October and 2009 January. These observations allowed us to construct broadband spectra of the sources in the low $\gamma$-ray activity state, covering optical to GeV photon energy range. Our results are as follows.

1. The X-ray spectra of five FSRQs are well represented by an absorbed hard power-law model ($\Gamma \sim 1.4$–1.7). For PKS 0208−512, PKS 1127−145, and 3C 454.3, the fitted absorption column is larger than the Galactic value (but we note that the "excess absorption" is not a unique representation of X-ray spectra of those blazars). Compared with

previous X-ray observations, we see a trend of increasing apparent X-ray absorption column with increasing high-energy luminosity of the source.
2. *Suzaku* observations reveal spectral evolution of the X-ray emission: the X-ray spectrum becomes harder as the source gets brighter. Such spectral changes are most likely due to the underlying and steady low-energy spectral component which becomes prominent when the IC emission gets fainter. This soft X-ray excess can be explained as a contribution of the high-energy tail of the synchrotron component, or bulk-Compton radiation.
3. We adopt the location of the blazar emission region to be outside of the immediate vicinity of the accretion disk but within the BLR, and within the context of this model, we find that the contribution of the synchrotron SSC process to the high-energy radiative output of FSRQs is negligible even in their low-activity states.
4. We argue that the difference between the low- and high-activity states in luminous blazars is due to the different total kinetic power of the jet, most likely related to varying bulk Lorentz factor of the outflow within the blazar emission zone.

The *Fermi* LAT Collaboration acknowledges generous ongoing support from a number of agencies and institutes that have supported both the development and the operation of the LAT as well as scientific data analysis. These include the National Aeronautics and Space Administration and the Department of Energy in the United States, the Commissariat à l'Energie Atomique and the Centre National de la Recherche Scientifique/Institut National de Physique Nucléaire et de Physique des Particules in France, the Agenzia Spaziale Italiana and the Istituto Nazionale di Fisica Nucleare in Italy, the Ministry of Education, Culture, Sports, Science and Technology (MEXT), High Energy Accelerator Research Organization (KEK), and Japan Aerospace Exploration Agency (JAXA) in Japan, and the K. A. Wallenberg Foundation, the Swedish Research Council, and the Swedish National Space Board in Sweden.

Additional support for science analysis during the operations phase is gratefully acknowledged from the Istituto Nazionale di Astrofisica in Italy and the Centre National d'Études Spatiales in France.

Ł.S. was partially supported by the Polish Ministry of Science and Higher Education through the project N N203 380336.

## REFERENCES

Abdo, A. A., et al. 2009a, ApJS, 183, 46
Abdo, A. A., et al. 2009b, ApJ, 700, 597
Abdo, A. A., et al. 2009c, ApJ, 699, 31
Abdo, A. A., et al. 2010, ApJ, 710, 1271
Amato, E., & Arons, J. 2006, ApJ, 653, 325
Atwood, W. B., et al. 2009, ApJ, 697, 1071
Barthelmy, S. D., et al. 2005, Space Sci. Rev., 120, 143
Bechtold, J., Siemiginowska, A., Aldcroft, T. L., Elvis, M., & Dobrzycki, A. 2001, ApJ, 562, 133
Begelman, M. C., & Sikora, M. 1987, ApJ, 322, 650
Błażejowski, M., Siemiginowska, A., Sikora, M., Moderski, R., & Bechtold, J. 2004, ApJ, 600, L27
Błażejowski, M., Sikora, M., Moderski, R., & Madejski, G. M. 2000, ApJ, 545, 107
Burrows, D. N., et al. 2005, Space Sci. Rev., 120, 165
Cardelli, J. A., Clayton, G. C., & Mathis, J. S. 1989, ApJ, 345, 245
Celotti, A., Ghisellini, G., & Fabian, A. C. 2007, MNRAS, 375, 417
Dermer, C. D., & Schlickeiser, R. 1993, ApJ, 416, 458
Dickey, J. M., & Lockman, F. J. 1990, ARA&A, 28, 215
Donnarumma, I., et al. 2009, ApJ, 707, 1115
Edelson, R., Griffiths, G., Markowitz, A., Sembay, S., Turner, M. J. L., & Warwick, R. 2001, ApJ, 554, 274
Foschini, L., et al. 2006, A&A, 453, 829
Fukazawa, Y., et al. 2006, Proc. SPIE, 6266, 75
Ghisellini, G., Celotti, A., Fossati, G., Maraschi, L., & Comastri, A. 1998, MNRAS, 301, 451
Ghisellini, G., Tavecchio, F., & Ghirlanda, G. 2009, MNRAS, 399, 2041
Giommi, P., et al. 2006, A&A, 456, 911
Hartman, R. C., et al. 1999, ApJS, 123, 79
Hill, J., et al. 2004, APS, 10005H
Hoshino, A., Arons, J., Gallant, Y. A., & Langdon, A. B. 1992, ApJ, 390, 454
Jorstad, S. G., & Marscher, A. P. 2004, ApJ, 614, 615
Kataoka, J., et al. 1999, ApJ, 514, 138
Kataoka, J., et al. 2008, ApJ, 672, 787
Kokubun, M., et al. 2007, PASJ, 59, S53
Koyama, K., et al. 2007, PASJ, 59, S23
Maraschi, L., Ghisellini, G., & Celotti, A. 1992, ApJ, 397, L5
Mitsuda, K., et al. 2007, PASJ, 59, S1
Moderski, R., Sikora, M., Madejski, G. M., & Kamae, T. 2004, ApJ, 611, 770
Mukherjee, R., et al. 1999, ApJ, 527, 133
Murphy, E. M., Lockman, F. J., Laor, A., & Elvis, M. 1996, ApJS, 105, 369
Poole, T. S., et al. 2008, MNRAS, 383, 627
Raiteri, C. M., et al. 2007, A&A, 473, 819
Raiteri, C. M., et al. 2008, A&A, 491, 755
Roming, P. W. A., et al. 2005, Spacs Sci. Rev., 120, 95
Sambruna, R. M., Gliozzi, M., Tavecchio, F., Maraschi, L., & Foschini, L. 2006, ApJ, 652, 146
Sambruna, R. M., et al. 1997, ApJ, 474, 639
Schlegel, D. J., Finkbeiner, D. P., & Davis, M. 1998, ApJ, 500, 525
Serlemitsos, P. J., et al. 2007, PASJ, 59, S9
Sikora, M., Begelman, M. C., & Rees, M. J. 1994, ApJ, 421, 153
Sikora, M., & Madejski, G. M. 2000, ApJS, 534, 109
Sikora, M., Moderski, R., & Madejski, G. M. 2008, ApJ, 675, 71
Sikora, M., Stawarz, Ł., Moderski, R., Nalewajko, K., & Madejski, G. 2009, ApJ, 704, 38
Sokolov, A., & Marscher, A. P. 2005, ApJ, 629, 52
Takahashi, T., et al. 2007, PASJ, 59, S35
Tavecchio, F., & Ghisellini, G. 2008, MNRAS, 386, 945
Tavecchio, F., Maraschi, L., Ghisellini, G., Kataoka, J., Foschini, L., Sambruna, R. M., & Tagliaferri, G. 2007, ApJ, 665, 980
Tavecchio, F., et al. 2000, ApJ, 543, 535
Tavecchio, F., et al. 2002, ApJ, 575, 137
Thompson, D. J., et al. 1993, ApJS, 86, 629
Villata, M., et al. 2006, A&A, 453, 817